Journal of Hydrology: Regional Studies 36 (2021) 100877

Contents lists available at ScienceDirect

Journal of Hydrology: Regional Studies

journal homepage: www.elsevier.com/locate/ejrh

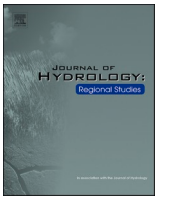

Effects of drought on groundwater-fed lake areas in the Nebraska Sand Hills

Nawaraj Shrestha [a], Aaron R. Mittelstet [b,*], Troy E. Gilmore [a], Vitaly Zlotnik [c], Christopher M. Neale [d]

[a] School of Natural Resources, University of Nebraska-Lincoln, Lincoln, NE, 68583, USA
[b] Biological Systems Engineering Department, University of Nebraska-Lincoln, Lincoln, NE, 68583, USA
[c] Department of Earth and Atmospheric Sciences, University of Nebraska-Lincoln, Lincoln, NE, 68588, USA
[d] Daugherty Water for Food Global Institute, University of Nebraska (UNL), Nebraska Innovation Campus, 2021 Transformation Dr. Ste 3220, Lincoln, NE, 68588, USA

ARTICLE INFO

Keywords:
Lake area
Palmer drought severity index
Drought
Remote sensing
Nebraska Sand Hills

ABSTRACT

Study region: The Nebraska Sand Hills (NSH) lies in the western part of Nebraska, United States. We chose the north-eastern, central, and western parts of NSH with distinct climate, topography, and hydrology.
Study focus: The study assesses the response of hundreds of shallow groundwater-fed lakes to drought. Total lake area (TLA), determined by classifying Landsat satellite images from 1984 to 2018, was juxtaposed with published Palmer Drought Severity Index (PDSI) and detrended cumulative PDSI (DeCumPDSI) at monthly and annual timescales. The PDSI and DeCumPDSI were time lagged to incorporate the preceding climatic effect (groundwater time lag) and evaluated against TLA using Bayesian regression analysis.
New hydrologic insight for the region: TLA in the NSH respond to the seasonal as well as long-term climatic effects moderated by topography, surface, and subsurface hydrology. A higher determination coefficient R^2 and lower mean square error of TLA at annual PDSI and DeCumPDSI illustrate the effect of long-term climatic fluctuations and groundwater influence: the evaporative losses from lakes are modulated by the lake-groundwater exchange, but the groundwater recharge has a longer response time to the drought. The study provides a simple method of assessment of the climate impact that results from the satellite data, gridded climate observation, and statistics for sensitive landscape of the NSH.

1. Introduction

Drought is a natural phenomenon that has severe socioeconomic and environmental effects (Ding et al., 2011; Mo et al., 2009). A decrease in rainfall duration, amount, and frequency causes drought to stress all components of a hydrologic system (Peters et al., 2006). The effects of drought are hard to characterize as drought propagates and produces responses at multiple spatial and temporal

Abbreviations: PDSI, Palmer Drought Severity Index; CumPDSI, Cumulative Palmer Drought Severity Index; DeCumPDSI, Detrended Cumulative Palmer Drought Severity Index.

* Corresponding author.
E-mail address: amittelstet2@unl.edu (A.R. Mittelstet).

https://doi.org/10.1016/j.ejrh.2021.100877
Received 16 November 2020; Received in revised form 13 July 2021; Accepted 20 July 2021
Available online 28 July 2021

scales. For example, a hydrologic system with hydraulic connectivity to groundwater produces a different response than a system without the connection (Peters et al., 2006). However, the effects of drought on the hydrological system can be characterized through the response of water bodies (e.g., lakes). Lake properties such as surface area, water level, volume, and salinity provide valuable information to assess the effect of drought on surface and groundwater hydrology (Tweed et al., 2009). The change in lake surface area, measured through remote sensing, helps to monitor and assess the response of the hydrologic system to drought. However, studies that quantify the response of thousands of shallow closed groundwater-fed lakes are limited.

Lakes are sensitive indicators of drought as they respond rapidly and integrate information about changes in environmental, landscape, and atmospheric conditions (Adrian et al., 2009; Harris, 1994; Mason et al., 1994; Pham et al., 2008; Williamson et al., 2008). The change in a lake's physical (Du et al., 2012; Li et al., 2018; Mason et al., 1994; Tang et al., 2018; Wang et al., 2018b; Yan and Zheng, 2015), biological (biota) (Williamson et al., 2008) or chemical (salinity) (Pham et al., 2008) characteristics help to explain the hydrologic response to drought. For example, Mason et al. (1994) found that the lake water level and size (surface area) are sensitive to low frequency climate signals (e.g. drought) but are less sensitive to high frequency climate signals (e.g. seasonal variations). Zhang et al. (2009) found that the lake responses are defined by the size. Large lakes respond to long-term climate effects but moderate the seasonal effects, while smaller lakes are sensitive and responsive to seasonal effects. In addition to climate, the response of lakes is regulated by contribution of the lake-groundwater exchange (Fig. 1), geographic regions (Adrian et al., 2009; Liao et al., 2013; Tang et al., 2018; Yan and Zheng, 2015), lake position relative to regional groundwater flow (Smith and Townley, 2002), drought severity and hydraulic connectivity (Peters et al., 2006; Pham et al., 2008; Tweed et al., 2009). Lakes with hydraulic connection to groundwater also provide the opportunity to evaluate or monitor the groundwater level variations. However, most of the studies have been focused previously on areas where lake hydrology is defined by a combination of precipitation, evaporation, and overland flow (Fig. 1a). Lakes water budget that include substantial surface water-groundwater exchange (Fig. 1b) respond differently asthe influence of surface water evaporation on lake water levels is compensated partially by the groundwater inflow fluxes and are less studied. However, these fluxes commonly lag behind the evaporative losses because they originate from groundwater recharge over large surrounding areas with long travel times through the hosting aquifer. Time lag, the time a precipitation event takes to travel through the subsurface and effect the lake area, is often used. For example, the present volume, number, and stage of lakes were determined by backward time averaging of climate events (Gong et al., 2015; Langbein, 1961; Liu and Schwartz, 2012; Mason et al., 1994).

Previous studies have primarily focused on lake water level and salinity to characterize the response from drought (Gosselin et al., 2000; Tweed et al., 2009). Fewer studies use lakes area to characterize the response of drought on water bodies. Lakes area, however, is easily quantified using remote sensing that provides opportunity to monitor lakes in remote areas with sparse or no observations. Remote sensing is an easily implemented method to delineate water surface area using single-band thresholding, classification, multi-band, and subpixel methods (Bijeesh and Narasimhamurthy, 2020; Du et al., 2012). Thresholding, the simplest method, involves selecting a threshold value to delineate water from single bands. However, the method suffers from errors such as mixing of water pixels with shadows due to overlapping of spectral signatures (Frazier and Page, 2000), along with a subjective selection of threshold values (Xu, 2006). The classification-based method uses all or some of the available bands to label classes with algorithms such as nearest neighborhood, maximum likelihood, ISO data, K-means, support vector machine, random forest, and artificial neural network to identify water area (Paul et al., 2018). The classification-based method usually serves as a better method than thresholding but suffers from a mixed pixel effect (Frazier and Page, 2000). Hybrid methods combine multiple methods to delineate and differentiate water areas. For example, multi-band images when combined with image color space (Jiang et al., 2012), principal component analysis (Balázs et al., 2018) or tasseled cap transformation (Hoan et al., 2012; Zhuang and Chen, 2018), provides better characterization of the water surface area.

The objective of this study was to characterize the spatial and temporal response of hundreds of shallow groundwater-fed lakes in the Nebraska Sand Hills (NSH) to drought. The lakes area derived from Landsat images are juxtaposed with drought indices, and the responses of lakes area are assessed using Bayesian ridge regression analysis.

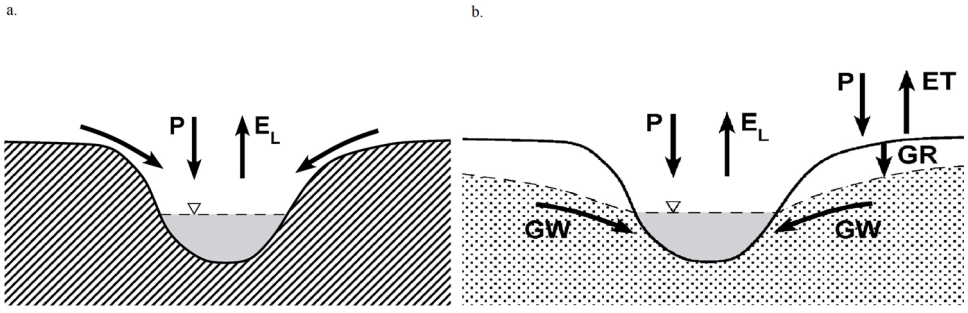

Fig. 1. Conceptual model of two extreme cases for shallow lakes: (a) lakes are imbedded in impermeable substrate and fed only by precipitation and overland flow; (b) lakes have hydraulic connection with groundwater; groundwater flux into the lake is the dominant component of inflow to the lake in the absence of overland flow.

2. Material and methods

2.1. Study area

The NSH is a drought-sensitive, grass stabilized eolian landscape, located in a semi-arid climate of western Nebraska (Fig. 2). Drought in the NSH, like in the entire United States (U.S.) are controlled by the low-frequency sea surface temperature anomalies in the Pacific and Atlantic Oceans (Mo and Lettenmaier, 2018; Schubert et al., 2004). The direct and indirect influence of the surface sea temperature anomalies in precipitation leads to a series of recurring and long-lasting drought in the NSH. The NSH is also vulnerable to drought due to semi-arid climate, eolian landscape, human encroachment and climate change (Adane et al., 2019; Burbach and Joeckel, 2006). The NSH has temperatures ranging from -40 to 43.3 °C with an average annual temperature of 8.9 °C. The annual average precipitation ranges from 450 mm in the west to 690 mm in the eastern part of NSH (National Climatic Data Center, 2020). The annual average precipitation ranges from 450 mm in the west to 690 mm in the east (National Climatic Data Center, 2020). Because of its semi-arid nature, a large proportion of precipitation is lost as evapotranspiration (> 700 mm) (Winter, 1986) and the groundwater influx makes up the difference. The sandy soils promote high infiltration with annual recharge rates of approximately 73 ± 73 mm yr^{-1}, varying between 40 ± 85 mm yr^{-1} in the western and 200 ± 85 mm yr^{-1} in the south-eastern parts (Szilagyi et al., 2011).

The combination of climate, topography, soil, and groundwater-surface water interactions resulted in a total of 4700 and 2000 km^2 of lakes and wetlands, respectively (Dappen et al., 2007). Most of the lakes are shallow with a depth less than 1 m while the lake areas range from 0.004–13 km^2 (Gosselin et al., 2000). The majority of the lakes are smaller than 0.2 km^2 (Table 1). Lake water level is lower than the regional groundwater level (Ong, 2010; Winter, 1986), and evapotranspiration that exceeds precipitation suggests that the lakes represent areas of focused groundwater discharge, typical for groundwater-fed lakes (Zlotnik et al., 2009). Given the difference in climate, topography, and lake density in the NSH, three study areas were selected for this research. The Western Lake Region (WLR) has the highest lake density of 0.035 per km^2 followed by the North-Eastern Region (NER) of 0.020 per km^2 and the Central Lake Region (CLR) 0.017 per km^2 (Fig. 2).

Geology is an integral part of the surface water and groundwater hydrology in the NSH. The dunes in NSH are composed of well-

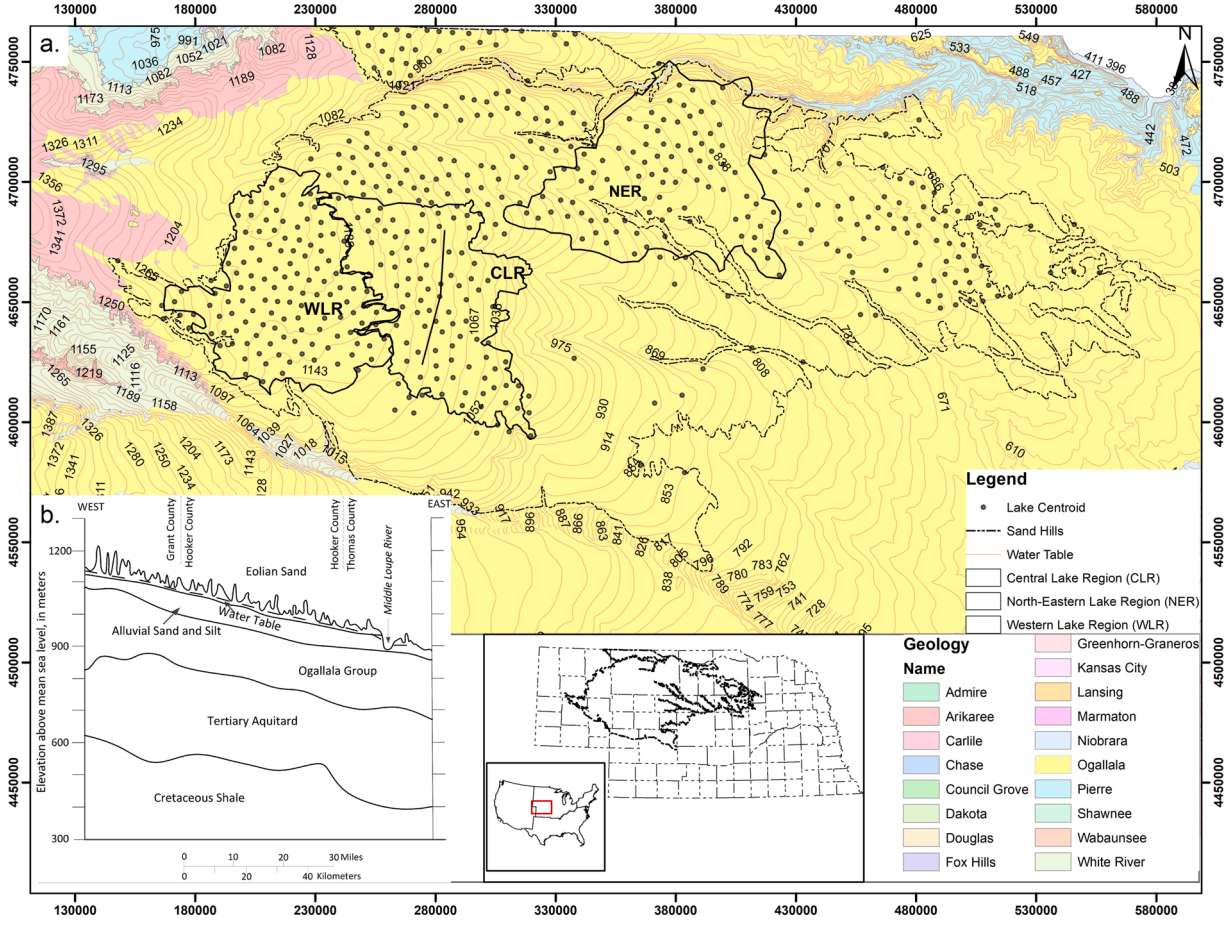

Fig. 2. The Ogallala group dominates the geology in the Western, Central and North-Eastern study area in the Nebraska Sand Hills (a), a cross-section shows geological formations present in the Nebraska Sand Hills (b) (Chen and Chen, 2004).

Table 1
Lake size distribution in the Nebraska Sand Hills.

Lake area (km^2)	Percentage
0–0.2	76.8
0.2–0.5	15.8
0.5–2	6.74
>2	0.717

sorted, fine to medium grained sand and lie atop the Quaternary deposits of alluvial sand and silt. The dunes and layer of alluvial sand and silt overlie the Ogallala Group are composed of moderate to low-permeable sand, sandstone, and siltstones (Fig. 2b). The dunes and Quaternary deposits have the highest permeability and form an important part of the aquifer through efficient transmission of recharge and minimizing evapotranspiration loss (Gutentag et al., 1984; Peterson et al., 2020). The Ogallala Formation, although less permeable, contains most of the groundwater due to considerable thickness and extent. The aquifer gently dips eastward at 0.9–1.3 m per km (Gutentag et al., 1984) and is part of the High Plains Aquifer system, where saturated. The Arikaree Formation and the White River Group lie beneath the Ogallala Group and are also part of the High Plains aquifer, though they are finer grained, and only contain usable quantities of water locally in fractured or coarse-grained areas.

2.2. Data

Landsat satellite images from three different sensors were used to extract the total lake area (TLA) (Table 2). Throughout the manuscript, TLA will refer to the area of all the lakes within the study area. The surface reflectance data from the Landsat Thematic Mapper (TM), Enhanced Thematic Mapper Plus (ETM+), and Operational Land Imager (OLI) with a similar spectral and spatial resolution in the multispectral region (Table 2) were used. The surface reflectance data, hosted in Google Earth Engine (GEE), were corrected for atmospheric and geometric effects using the LaSRC approach (Vermote et al., 2016). In this study, we used 450 images for the three-study areas. The monthly and annual distribution of images (Fig. 3) shows an uneven distribution. The highest number of images was available for September, October, and July. Annually, 2012 had the largest number of images for NER and 2016 for CLR and WLR.

Palmer drought severity index (PDSI) is calculated on the concept of water supply and demand. It uses precipitation, soil moisture content, potential evapotranspiration, water storage, runoff, and antecedent conditions to estimate soil moisture balance (Alley, 1984). The magnitude of drought is specified based on values ranging from −10 (dry) to +10 (wet) with values less than -3 indicating moderate to severe drought condition. PDSI is one of the widely used drought indices and provides a robust approximation of soil moisture variability as compared with other metrics such as the standardized precipitation evapotranspiration index (SPEI) (Cook et al., 2014). The use of precipitation and temperature from antecedent conditions provides better estimates of the soil water balance and the effect of water stress in the hydrological system (eg., soil moisture, streamflow) (Dai et al., 2004) than the indices that only consider precipitation or temperature (Keyantash et al., 2002). Similarly, the effects of warming due to climate change is better approximated by PDSI as compared with standardized precipitation index (SPI) (Dubrovsky et al., 2009). With a large proportion of precipitation lost to evapotranspiration and a high contribution from groundwater, soil moisture balance is an important component, and PDSI, therefore, provides proper representation of the drought conditions in the NSH.

The PDSI used in our study is calculated per-pixel (~ 4 km), with gridded meteorological data from the Parameter-elevation Regression on Independent Slopes Model (PRISM). The Penman-Montieth equation is used to calculate potential evapotranspiration while available soil water holding capacity in the top 2.5 m of the soil was derived from the STATSGO soils database. The PDSI data are available three times a month and were resampled for a monthly and annual series. Details on the method and data are provided in Abatzoglou et al. (2014).

Table 2
Landsat sensors and their spatial and spectral characteristics in the multispectral region.

Satellite	Sensor	Year	Resolution (m)	Wavelength (μm)
Landsat 4–5	Thematic Mapper (TM)	1984–2011	30	Band 1: 0.45–0.51 Band 2: 0.52–0.60 Band 3: 0.63–0.69 Band 4: 0.75–0.90 Band 5: 1.55–1.75 Band 7: 2.09–2.35
Landsat 7	Enhanced Thematic Mapper Plus (ETM+)	2012	30	Band 1: 0.43–0.45 Band 2: 0.45–0.51 Band 3: 0.53–0.59 Band 4: 0.63–0.67 Band 5: 0.85–0.87 Band 6: 1.56–1.65 Band 7: 2.10–2.29 Band 8: 0.50–0.67 Band 9: 1.36–1.38
Landsat 8	Operational Land Imager (OLI)	2013–2018	30	

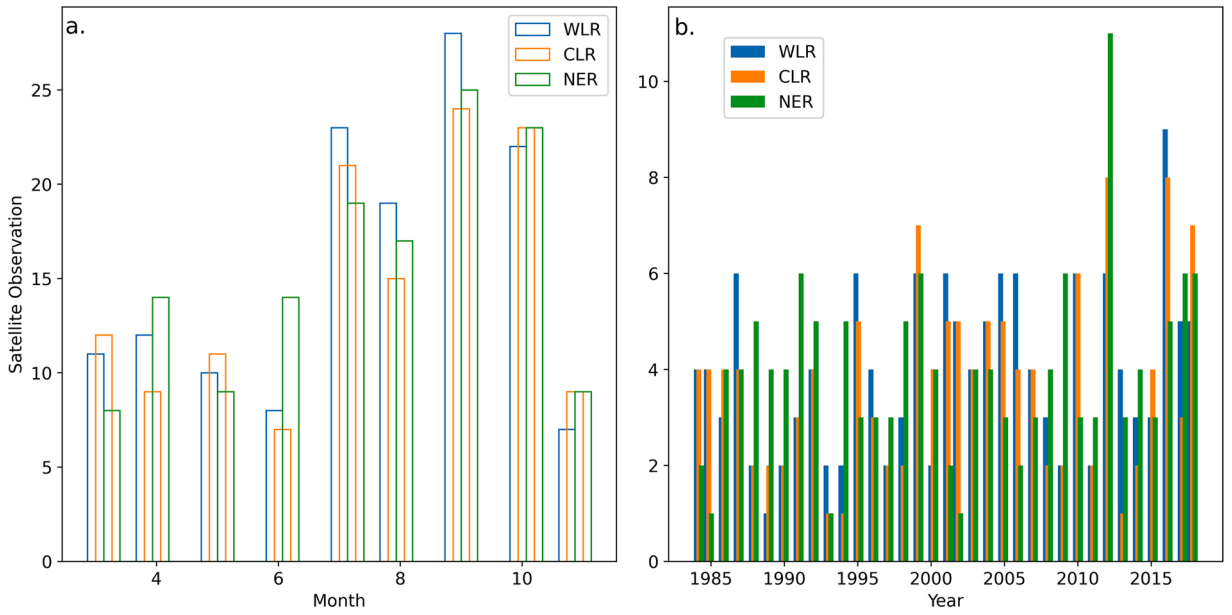

Fig. 3. Monthly and annual Landsat image distribution in the Western, Central, and North-Eastern Lake region.

2.3. Lake area extraction

The Landsat images (1984–2018), hosted in GEE, were filtered for cloud cover less than 10 %, and winter months (December-February) to reduce the effect of cloud and snow-covered lakes. Although NSH has a higher contrast ratio between water bodies and the surrounding land, high suspended sediment, submerged or floating vegetation and background reflectance from shallow water areas causes a mixed spectral response. The collection of images was therefore transformed using the tasseled cap transformation and combined with original bands to capture spectral variability present in the NSH. Tasseled cap transformation uses empirical coefficients (Baig et al., 2014; Crist and Cicone, 1984; Huang et al., 2002) to derive components, where the first three components, brightness, greenness, and wetness, account for the most variation (Crist and Kauth, 1986). The wetness feature is sensitive to soil and plant moisture and reduces the influence of shadows and enhances water body detection and delineation (Hoan et al., 2012; Jain et al., 2005; Zhuang and Chen, 2018). The greenness, wetness, and brightness components of tasseled cap transformation were stacked with original bands and a random forest classifier in GEE was used to classify the images into water and non-water areas. Training samples were collected from the water bodies (150) and non-water (200) areas using visual analysis. Random forest classifier, an ensemble of decision trees that provides higher accuracy and is widely used in processing remotely sensed imagery including water and wetland classification (Tian et al., 2016; Wang et al., 2018a, 2020), was used to classify the time series images. Water areas consisting of a limited number of pixels are mainly associated with image misclassification due to mixed pixel effects, therefore, areas with less than 10 pixels were removed using a majority filter with eight neighborhoods, i.e., a kernel of 3×3 pixels. As a result of filtering, any object smaller than 0.81 ha (0.0081 km^2) was automatically removed from the data.

The gaps present in the lakes from Landsat ETM + sensor was filled using the nibble tool in ArcGIS Pro 2.4. The scan line corrector (SLC) error present in ETM + images were extracted and reclassified as NoData to define a mask raster. The nibble operation then grows the lake area (input cells) into the nearest NoData cells of the mask raster. The shape and area of the lakes are preserved as it only fills the missing pixels within the neighborhood defined in the mask raster. As the PDSI has spatial resolution of 4 km, the response of individual lakes was not properly differentiable, therefore, we summed the lakes area (TLA) within each study area for further analysis. This also averages the uncertainty associated with smaller lakes undetected and removed during the classification process.

2.4. PDSI and total lake area time series

Lakes in the NSH are primarily groundwater-fed and lake dynamics are a function of the current and preceding climatic conditions. To account for the dependence of TLA on hydrologic conditions in preceding years, a cumulative PDSI (CumPDSI) was derived (Eq.1).

$$CumPDSI_k = \sum_{n=1}^{k} PDSI_k \tag{1}$$

where, $CumPDSI_k$ is the cumulative PDSI values by k-th time, and $PDSI_k$ is PDSI value at the k-th time and is calculated monthly, and annually.

PDSI, a water-balance index when summed (CumPDSI) should have a trend with a slope of zero over the long-term. However, the

CumPDSI exhibited a trend, which was removed (Fig. 4) to calculate detrended PDSI (DePDSI) and detrended cumulative PDSI (DeCumPDSI) (Huang et al., 2011) using Eqs. 2 and 3 respectively. The trends were calculated using a simple linear regression that uses least squares to minimize the difference between the observed and fitted values. The slope of the regression was then used to remove the trend present in PDSI. A negative trend in WLR, CLR, and NER was removed by adding a value of 0.1330, 0.2078, and 0.2340 respectively. The values inside square brackets (Eq. 2) indicate respective trend values in CLR and NER region.

$$DePDSI_k = PDSI_k + [0.133, +0.2078, +0.234] \tag{2}$$

where, k ranges from *1* to *n*. In analogy with $CumPDSI_k$, a detrended cumulative index $DeCumPDSI_k$ was calculated using Eq.3. The PDSI and DeCumPDSI were aggregated for monthly and annual timescale.

$$DeCumPDSI_k = \sum_{n=1}^{k} DePDSI_k \tag{3}$$

2.5. Total lake area and PDSI regression analysis

The Bayesian ridge regression was used to predict the response of TLA in the NSH. The PDSI and DeCumPDSI were time lagged by t to incorporate effects of groundwater influence from drought. The Bayesian ridge regression uses the probability distribution of the independent variable and its coefficients to estimate the distribution of the dependent variable (Murphy, 2012). Assuming a Gaussian distribution, the response is estimated as:

$$y \sim N(\mu,\ \alpha^{-1}) \tag{4}$$

where $y = \{y_1, y_{2.....}\ y_n\}$ is the dependent variable (TLA) parametrized by mean $\mu = X\omega$ and variance α^{-1}. X is n*m matrix of time lagged PDSI, or DeCumPDSI and ω is the weight.

The Bayesian approach computes posterior distribution $p(\omega|y,X) \alpha p(y|\omega,X) \times p(\omega,X)$ as a product of likelihood and prior distribution. The prior distribution is given by spherical Gaussian centered about zero, $\omega \sim \mathcal{N}(0,\ \lambda^{-1}\mathrm{I})$ The priors for α^{-1} and λ^{-1} are gamma distributions, i.e., $\alpha \sim\ G(\alpha_1, \alpha_1)$, $\lambda \sim G(\lambda_1, \lambda_2)$, and $\alpha > 0$, $\lambda > 0$. α, λ, and ω are estimated from the data during training process (Bishop, 2006). The λ also serves as a regularization parameter which is estimated from the data during the training phase, eliminates subjectivity and makes the algorithm more stable. The ridge regression reduces the effect of collinearity and thereby avoids high prediction error associated with correlated data (Murphy, 2012). Because the posterior distribution is Gaussian, its mode coincides with mean, and therefore maximum posterior is calculated to minimize the prediction loss. Maximization of the posterior distribution with respect to weights ω minimizes the sum-of-squares with the addition of the quadratic minimization parameter λ (Eq. 5).

$$\widehat{\omega}_{MAP} = (X^T X + \lambda \mathbb{I}\ )^{-1}\ X^T Y \tag{5}$$

where X is the matrix of inputs and $\mathbb{I}$ is the identity matrix.

The dependent variables are then solved using Eq. 6 to get the estimate of the lakes sizes.

$$\widehat{Y} = X(X^T X + \lambda \mathbb{I}\ )^{-1}\ X^T Y \tag{6}$$

To determine the number of preceding climatic events that define the TLA, a correlation and a regression analysis between the TLA and time lagged PDSI and DeCumPDSI were performed. The PDSI and DeCumPDSI were time lagged to thirty-six past observations, corresponding to the three and thirty-six years for monthly and annual data. PDSI and DeCumPDSI from the past were combined

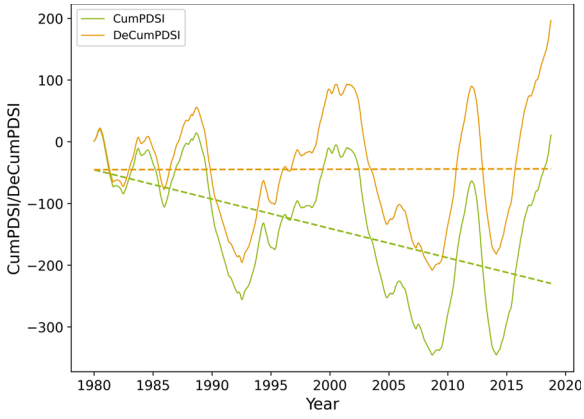

Fig. 4. The relation between PDSI with cumulative PDSI (CumPDSI) and detrended cumulative PDSI (DeCumPDSI). A negative trend present in CumPDSI is removed to calculate the DeCumPDSI.

sequentially and a regression analysis was evaluated using R^2. The performance (R^2) was plotted against the features (Fig. 5). A combination that produced the highest R^2 and lowest MSE was selected as the final model.

The α and λ parameters of the Bayesian regression are random numbers that follow the gamma distribution and are estimated during the training process. A grid search cross validation method was used to estimate the optimal α and λ values. The values [10^{-3}, 10^{-4}, 10^{-5}, 10^{-6}, 10^{-7}, 10^{-8}, 10^{-10}, 10^{-12}, 10^{-15}] were used to find the optimal parameters. The results (Fig. 6) shows that the negative mean squared errors do not change significantly with lower hyper-parameters values (10^{-6}). Therefore, the default values of $\alpha_1=\alpha_{2=}$ $\lambda_1=\lambda_2=10^{-6}$ as suggested by MacKay (1992) were used as the Bayesian ridge regression is insensitive to hyper-parameter settings. We used 70 % of the data to train and 30 % to test the model using the Scikit-Learn (Pedregosa et al., 2011) package implemented in Python 3.7.

Effect of irrigation on groundwater level and its subsequent effect on the TLA were analyzed using hotspot analysis of active irrigation well data hosted by the Conservation and Survey Division, School of Natural Resources, University of Nebraska-Lincoln, and the Nebraska Department of Natural Resources (Conservation and Survey Division, 2021a). Hotspot analysis, performed using ArcGIS Pro 2.6, shows if the underlying spatial pattern is significant or the result is from random processes (Getis and Ord, 1992; Scott and Janikas, 2010). It creates statistically significant spatial clusters of high or low values with z-score, p-value, and confidence level. A high z-score with small p-value indicate spatial clustering of high values while a low negative z-score and small p-value indicate a spatial clustering of low values (Scott and Janikas, 2010). In our study we used the location of irrigation wells to calculate the zones with higher and lower pumping rates.

A convergence index (Conrad et al., 2015) was calculated from the digital elevation model with a resolution of 30 m to highlight the effect of topography on TLA response. The calculation uses aspect and finds the degree to which the surrounding cells point to the center cell. The convergence index with values of zero indicate a planar (valley), a negative value shows a convergent (channels), and a positive value indicate divergent (ridges) surface (Conrad et al., 2015).

2.6. Accuracy assessment

Accuracy of the extracted lakes was assessed using high spatial resolution aerial images from the National Agriculture Imagery Program (NAIP) as reference data. Images were selected to represent the normal, dry, and wet seasons based on the availability of NAIP and cloud-free Landsat images. We used three different years to represent TLA variation during normal (2004), dry (2012), and wet (2018) years. For each year, 100 random points were generated using a random point algorithm and labeled using visual interpretation in GEE. The overall accuracy, error of commission, omission, and Kappa statistics were calculated. The error of commission represents the percentage of pixels classified as lakes that do not belong to the lakes as per the reference NAIP data, while the error of omission is the percentage of the pixels that are present as lakes in the reference data, but absent in classified data. Kappa statistics show whether the results of the error matrix is significantly better than agreement due to chance (Stehman, 1997).

3. Results

3.1. Accuracy of lake area

The lake area extracted from Landsat images, when compared with NAIP, illustrates an overall accuracy greater than 95 % for the normal, dry, and wet years (Table 3). The error of commission and omission were less than 5 % and 8 %, respectively, for each year. The Kappa statistics greater than 93 % highlights that the lake area are significantly better than chance.

3.2. Relationship between PDSI and total lake area

A correlation analysis shows a strong cyclic pattern in TLA with annual PDSI and DeCumPDSI. A linear decrease in correlation is

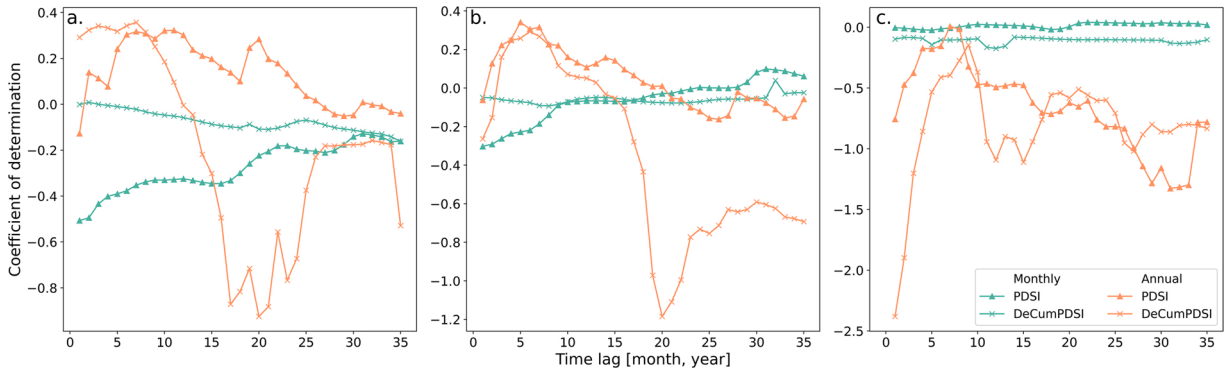

Fig. 5. The relationship between the total lake area and sequential time lagged PDSI and DeCumPDSI at Western Lake Region a), Central Lake Region b), and North-Eastern Lake Region c) at monthly and annual timescale.

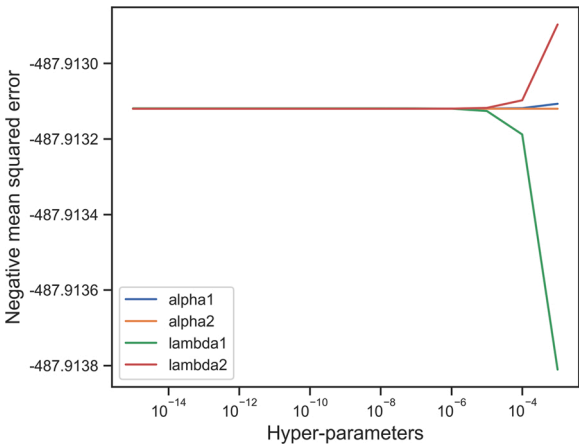

Fig. 6. Hyper-parameter sensitivity of α and λ in Bayesian ridge regression.

Table 3
Lake area accuracy in percentage for a normal (2004), dry (2012) and wet (2018) year as compared with National Agriculture Imagery Program images.

Accuracy Metrics	Year		
	2004	2012	2018
Overall	97	97	98
Commission	95	96	97
Omission	92	94	93
Kappa	93	95	95

seen in monthly PDSI while the DeCumPDSI displays a weaker cyclic pattern (Fig. 7). A linear and weaker cyclic pattern in correlation in monthly data indicates that the climate from the previous year contributes to the current TLA.

3.2.1. Spatial variation of total lake area

A long-term average of classified lakes from 1984 to 2018 shows a spatial pattern in TLA variation. Since the classified image had a value of 1 for presence and 0 for the absence of water, an area with a consistent presence of water has a mean value closer to 1, while an area with a value closer to 0 indicates the intermittent presence of water. Table 4 shows the percentage of TLA fluctuation between 1984 and 2018. NER has the highest percentage of lakes that fluctuates equal to or less than 20 % of the time while WLR shows the highest proportion of permanent lakes. Fig. 8 shows individual lakes differing responses to drought. Lake boundaries in the northern WLR (Fig. 8a) fluctuate more often than the lakes in the southern WLR (Fig. 8c). Some of the larger lakes in the NER are less variable, as the area is modified through human interference such as dams and irrigation.

The spatial pattern in TLA fluctuation is due to the variability in hydraulic conductivity, flow direction and the gradient of the regional groundwater. Apart from the influence of the underlying groundwater condition, the existence of lakes in the NSH is strongly controlled by topography. The fluctuation is pronounced when the lakes are present in the convergent and divergent topography

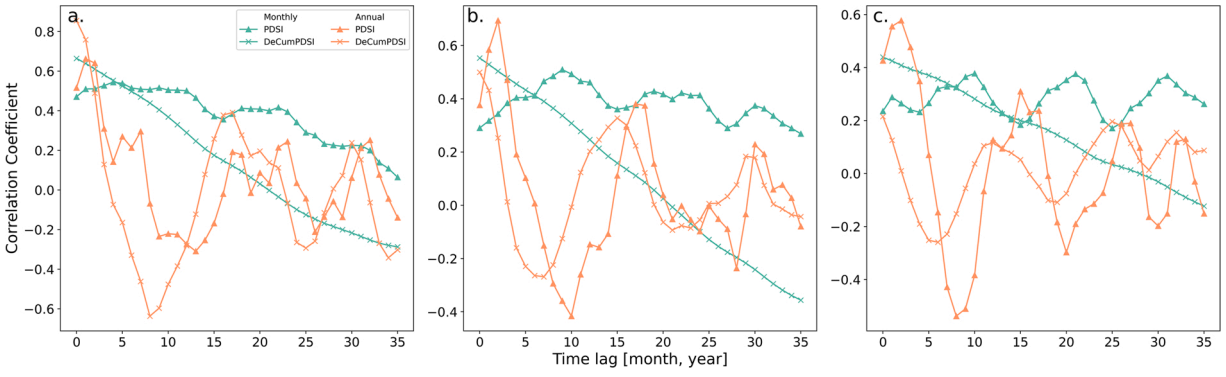

Fig. 7. Correlation between total lake area and time lagged PDSI and DeCumPDSI at Western a), Central b), and North-Eastern c) Lake Region at monthly and annual timescale.

Table 4
Study area with percent change in total lake area (TLA) from 1984-2018 in the Western, Central, and North-Eastern lake region.

% Change in TLA	Study area		
	WLR	CLR	NER
< 20	48.46	58.43	61.20
20–40	9.48	10.17	5.38
40–60	6.42	6.41	3.44
> 60	35.64	24.99	29.98

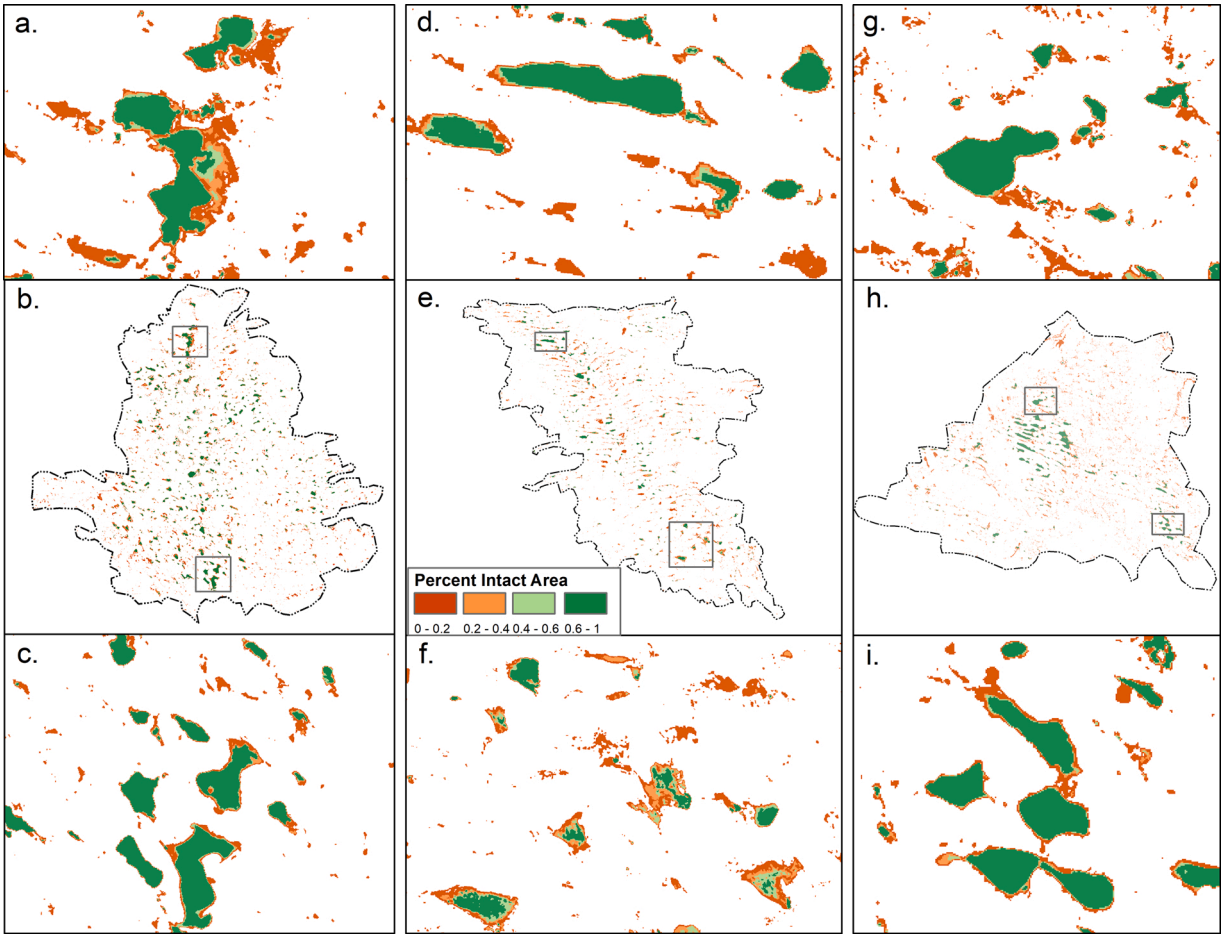

Fig. 8. Average lake area variation (1984-2018) in the Western (a, b, c), Central (d, e, f), and the North-Eastern (g, h, i) Lake region. Pixels with green color show the least variation while pixels with red show the highest variation. (For interpretation of the references to colour in this figure legend, the reader is referred to the web version of this article).

(Fig. 9). The lakes in planar areas are permanent (Fig. 9) indicating strong influence of topography.

The number of irrigation wells has increased dramatically in the last 80 years in the NSH. For example, irrigation wells increased from only a few hundred in 1940–7775 within a 10 km outside buffer of the NSH boundary in 2019 (Conservation and Survey Division, 2021b). The presence of hotspots near NER and modified lakes provides some explanation for the varied relation. A hotspot map (Fig. 10) shows that the lakes in NER have a higher chance of being influenced by irrigation. Smaller hotspot zones also lie closer to WLR, while the majority of the NSH lies on the cold spot or not significant zone indicating little or no interference of irrigation on groundwater and TLA (Fig. 10).

3.2.2. Temporal variation in total lake area

The temporal response of lakes in the NSH reveals seasonal, abrupt, and long-term effects of drought. The scattering of TLA, represented in Fig. 11, shows the effect of seasonal climatic variation. The smoothened (Savitzky-Golay filter) TLA variation,

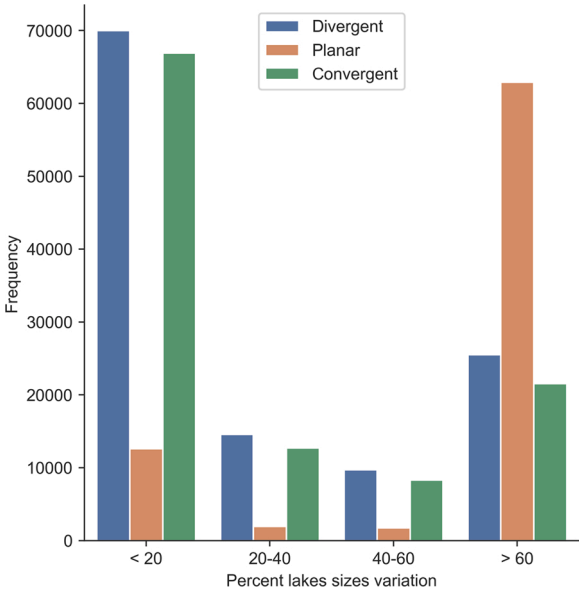

Fig. 9. A convergence index shows the occurrence of planar, divergent, and convergent topography in different percent of lakes area variation.

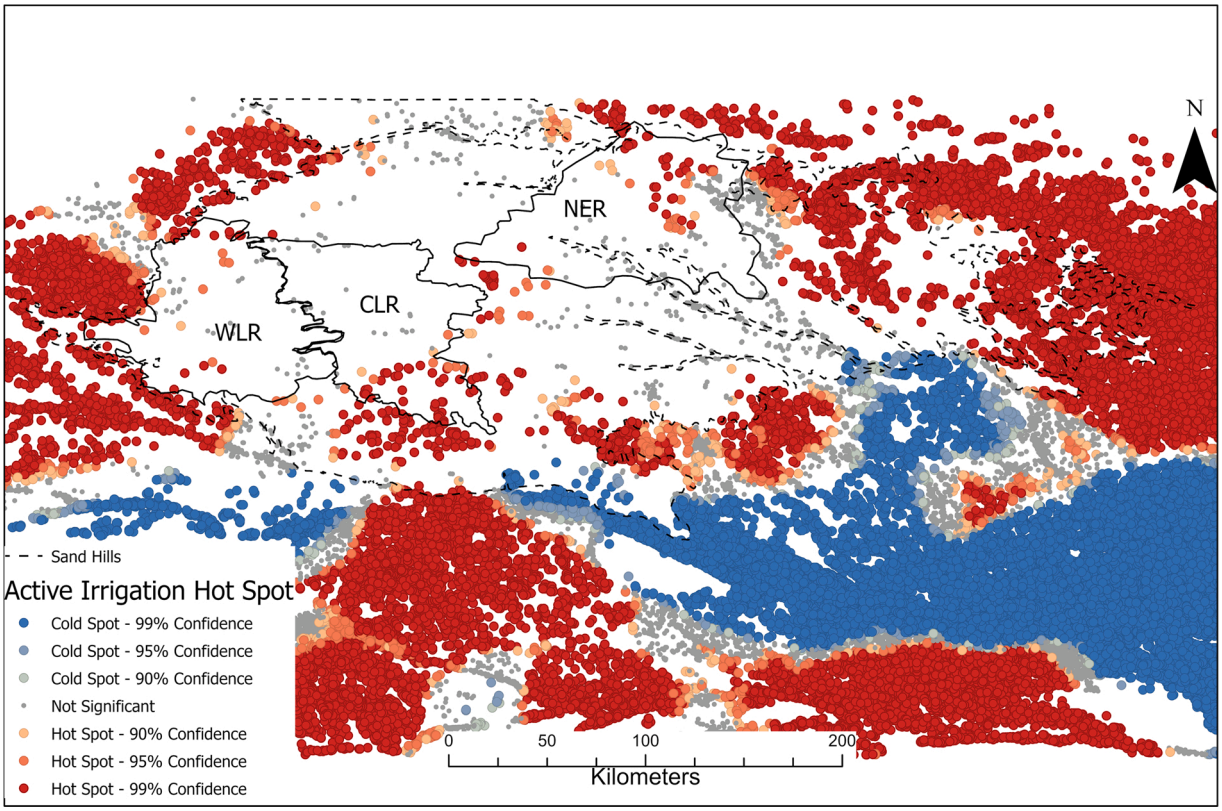

Fig. 10. Hot Spot analysis from the active irrigation wells show areas with the significant and non-significant clusters.

represented as a solid line in Fig. 11, illustrates the response of lakes to multiyear droughts. The multiyear drought of 2000–2005, for example, caused a considerable reduction in TLA. Similarly, an abrupt drought from May-August of 2012 drastically reduced the TLA. Fig. 11 also shows that the TLA fluctuation follows the Pacific Decadal Oscillation (PDO). It also highlights that the effect of PDO is not immediate. The TLA decreases after reductions in PDO for a few years and indicates the presence of lag in the response of lakes. This

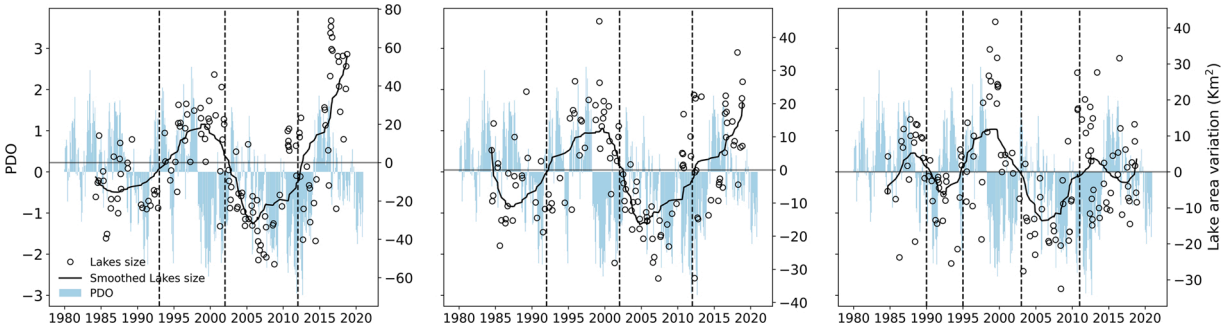

Fig. 11. Calculated and smoothed total lake area variation in the Western, Central, and North-Eastern Lake Region. The vertical lines show point of change, and open circles represent total lake area. The lake response shows delayed effect of Pacific Decadal Oscillation (PDO).

highlights that the TLA in the NSH depends on the groundwater flux and varying responses to drought. For example, lakes in WLR and CLR show a longer time lag while NER indicates a shorter time lag. The sensitivity of WLR can be due to the presence of a thicker vadose zone that promotes longer travel times for precipitation. NER less sensitive to immediate climate effects can be due to the gentle topography, consistent groundwater flux, or human interference such as irrigation (Fig. 10).

3.2.3. Lake response to drought

A Bayesian ridge regression model shows that the variations in TLA are best explained on an annual timescale (Figs. 12b, d, f). The relationship between the TLA and independent variables (PDSI and DeCumPDSI) is best demonstrated by DeCumPDSI in the WLR and CLR. The DeCumPDSI increased the R^2 and reduced the mean squared error (MSE) on the training and testing data at monthly and annual time series. The NER, however, showed a slightly better estimate with PDSI on monthly and annual data (Table 5).

Lower R^2 and higher MSE values at a monthly timescale (Fig. 12a, c, f) suggest that the TLA variation has higher uncertainty and less correlation than at a longer time scale. A lesser fitting could be related to the fact that smaller lakes (<0.8 ha) that respond rapidly to climatic fluctuations, removed to reduce the uncertainty, were not considered in the analysis. Similarly, seasonality in TLA may not be well represented due to the limited number of cloud and snow-free images. On an annual timescale, a high R^2 and low MSE is obtained using 5–10 years of time-lagged PDSI and DeCumPDSI values at all three study areas (Fig. 5a, b, c). Maximum MSE within four Landsat pixels shows that the annual DeCumPDSI could be used to determine the lake response in the NSH. In general, the R^2 values increases and MSE decreases for the PDSI and DeCumPDSI when the timescale is increased from monthly to annual. This suggests that the TLA variation in the NSH is controlled by the longer-term effect of drought and that the response time of lakes as modulated by groundwater flow is in terms of many years (5–10) instead of months and days.

4. Discussion

The TLA classified using the random forest classifier showed the highest accuracy. The higher accuracy (>95 %) is the result of a combination of tasseled cap components, original bands, and higher contrast between the water and homogenous surrounding landscape. With a spatial resolution of 30 m, at least 9 pixels are necessary to consistently represent an object using Landsat images (Ozesmi and Bauer, 2002). To avoid mixed pixel effect due to high suspended sediment, submerged or floating vegetation, and background reflectance at lake boundaries, pixels within 3*3 filters were removed. This leads to underrepresentation of the smaller lakes. Similarly, a unevenly distributed and limited number of cloud-free images resulted in the inability to capture the seasonal variation present in the TLA. The study, therefore, has partial or limited response of spatial and temporal variation of smaller lakes. The results, however, show that higher resolution satellites (e.g., Sentinel-2) could be used to characterize the smaller lakes and its response to seasonal variation. However, many higher resolution satellites have limited temporal (re-visit frequency) and shorter periods of records.

The lake hydrology in the NSH is dependent on the precipitation and groundwater fluxes as input, evapotranspiration as output, and little or no contribution from overland flow. The effect of precipitation is clearly seen as the TLA fluctuates in response to the seasonal and long-term climate changes. Although seasonal variations are not apparent, the long-term effects of climate fluctuations is seen in the time-series TLA and high R^2 values in Bayesian regression with annual data. The results correspond with several studies indicating that the climate in the central U.S. is the result of inter-annual and multiyear variation of the precipitation from air masses originating from the Pacific Ocean, the Arctic and the Gulf of Mexico (Bryson and Hare, 1974; Kushnir et al., 2010; Schubert et al., 2009). The sea surface temperature fluctuations cause shorter and longer oscillations of climate signals such as Quasi-Biennial Oscillation (QBO), El Niño-Southern Oscillation (ENSO), the Quasi-Decadal Oscillation (QDO), Atlantic Multidecadal Oscillation (AMO) and PDO (White et al., 2008). The PDO and AMO cause interdecadal oscillation and result in the long-term trend and decadal variability of drought in the central U.S. (Mo and Lettenmaier, 2018; Nigam et al., 2011; White et al., 2008). Fig. 11 illustrates that PDO affects the TLA in the NSH.

Groundwater plays an important role in the existence of lakes in the NSH. With evapotranspiration exceeding precipitation, the deficit in water budget of lakes is fulfilled by the groundwater contribution. The high coefficient of determination and low MSE with

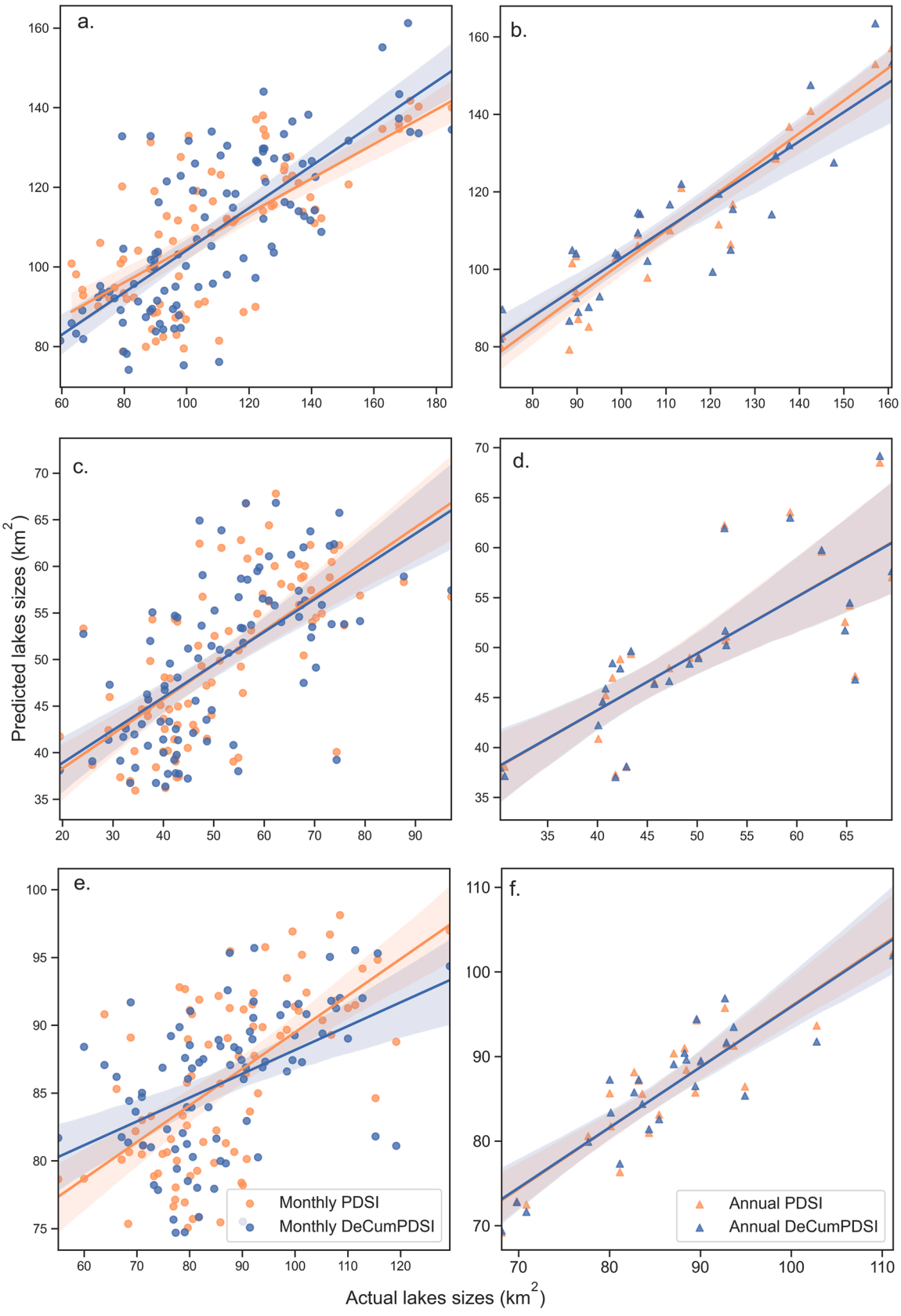

(caption on next page)

Fig. 12. Relationship between the actual and predicted total lake area in the Western (a, b), Central (c, d), and North-Eastern (e, f) Lake Region using PDSI, and DeCumPDSI at monthly and annual timescale.

Table 5
Performance of Bayesian ridge regression using time lagged Palmer Drought Severity Index (PDSI) and DeCumPDSI at Western, Central, and North-Eastern Lake Region at monthly and annual timescale. Values in square brackets correspond to test data.

		Monthly		Annual	
		R2	MSE	R2	MSE
WLR	PDSI	0.48, [0.48]	416, [358]	0.89, [0.46]	63, [247]
	DeCumPDSI	0.54, [0.57]	353, [315]	0.80, [0.86]	113, [53]
CLR	PDSI	0.41, [0.40]	132, [112]	0.61, [0.46]	50, [103]
	DeCumPDSI	0.37, [0.54]	141, [86]	0.60, [0.52]	51, [91]
NER	PDSI	0.34, [0.28]	135, [123]	0.79, [0.45]	19, [116]
	DeCumPDSI	0.21, [0.21]	162, [135]	0.77, [0.43]	20, [120]

time lagged annual data indicates the effect of groundwater in the lake response. The difference in the water table depth, vadose zone thickness, and hydraulic connectivity shows spatial and temporal patterns in TLA. The predominance of fine to coarse-grained sand permits high infiltration, thus leading to a shorter lag time and therefore the response time of the TLA. Our results from the WLR show a longer time lag than the NER and lies between 5–10 years. Besides precipitation and groundwater contribution, studies have shown the TLA also depends on the gradient of groundwater flow (Peters et al., 2006; Pham et al., 2008), position of lakes with respect to the local or regional groundwater flow (Tague et al., 2008), storage and lake bathymetry (Tweed et al., 2009) and topography. As evident in this study, local variation in hydraulic connectivity (Fig. 8a, d. vs Fig. 8c), topography (Fig. 9), and bathymetry results in immediate drying up of smaller shallow lakes and area reduction of larger or groundwater-fed lakes during drought. The results indicate that the TLA fluctuation can measure and monitor the groundwater level variation in the NSH.

Some of the differences in lower correlation and low R^2 between TLA and short-term climatic effects can also be attributed to the inherent drawbacks of PDSI. These include (i) the assumption of no runoff until the water capacity of the topsoil layer is full, while in the NSH, due to the high hydraulic conductivity of the sandy soil, the majority of the precipitation infiltrates and there may be little or no runoff, and (ii) exclusion of snow cover, snowfall, and frozen ground in PDSI calculation (Dracup, 1991), which is prevalent in winter months in the NSH and therefore might lead to some limitations in relation to the TLA. TLA, however, does not show significant variation in winter months due to low evaporation and, (iii) inability of PDSI to capture the climatic variability of a shorter temporal scale (less than 9-months) (Heim, 2002). Therefore, although PDSI best represents the soil moisture condition in NSH, other drought indices such as SPI, SPEI should be explored in future research.

The variations in lake responses in the NSH, because of local hydraulic conductivity, regional lake position, and topographic influences, can be refined in future studies. With few monitoring wells in the NSH, future work should also evaluate the potential in using the lakes as monitoring "wells" to better quantify the groundwater levels in the NSH.

5. Conclusions

This study presents the spatial and temporal TLA variation in response to climatic changes in the NSH. The spatial and temporal variations are apparent in TLA in response to the seasonal and longer-term climatic effects. The response of the lakes is controlled by the geographic location, the local variation of topography, climate, and groundwater influence. The longer response time, as determined by the higher degree of fit and lower MSE at the annual time scale using Bayesian analysis, shows that the groundwater is crucial in determining the response of lakes in the NSH. Similarly, a higher degree of fit with detrended cumulative PDSI highlights the importance of water balance and preceding climate effect on the lakes of the NSH.

The study, therefore, provides a simple and effective method to monitor and predict the lake response with readily available a priori climate data. The TLA, calculated with a limited number of cloud-free satellite images, however, may not represent the seasonal fluctuations in the NSH. Similarly, the response of smaller lakes that are sensitive to short-term climatic forcing may be biased due to the limited spatial resolution of the Landsat sensor.

Author statement

Nawaraj Shrestha: Data curation, Methodology, Formal analysis, Writing – Original Draft, Visualization. Aaron Mittelstet: Conceptualization, Writing – Review & Editing, Supervision, Funding acquisition. Troy E. Gilmore: Conceptualization, Writing – Review & Editing. Vitaly Zlotnik: Conceptualization, Writing – Review & Editing. Christopher Neale: Writing - Review & Editing.

Declaration of Competing Interest

The authors declare that they have no known competing financial interests or personal relationships that could have appeared to influence the work reported in this paper.

Acknowledgments

The authors acknowledge the U.S. Department of Agriculture - National Institute of Food and Agriculture (Hatch project 1015698), Robert B. Daugherty Water for Food Global Institute at the University of Nebraska-Lincoln and the Water Sustainability Fund, Nebraska Natural Resource Commission. The authors would thank the insgithful comments and suggestions from editors and anonymous reviewers for improving the quality of the manuscript.

Appendix A. Supplementary data

Supplementary material related to this article can be found, in the online version, at doi:https://doi.org/10.1016/j.ejrh.2021.100877.

References

Abatzoglou, J.T., Barbero, R., Wolf, J.W., Holden, Z.A., 2014. Tracking interannual streamflow variability with drought indices in the U.S. Pacific Northwest. J. Hydrometeorol. 15, 1900–1912. https://doi.org/10.1175/JHM-D-13-0167.1.

Adane, Z., Zlotnik, V.A., Rossman, N.R., Wang, T., Nasta, P., Adane, Z., Zlotnik, V.A., Rossman, N.R., Wang, T., Nasta, P., 2019. Sensitivity of potential groundwater recharge to projected climate change scenarios: a site-specific study in the Nebraska Sand Hills, USA. Water 11, 950. https://doi.org/10.3390/w11050950.

Adrian, R., O'Reilly, C.M., Zagarese, H., Baines, S.B., Hessen, D.O., Keller, W., Livingstone, D.M., Sommaruga, R., Straile, D., Van Donk, E., Weyhenmeyer, G.A., Winder, M., 2009. Lakes as sentinels of climate change. Limnol. Oceanogr. 54, 2283–2297. https://doi.org/10.4319/lo.2009.54.6_part_2.2283.

Alley, W.M., 1984. The palmer drought severity index: limitations and assumptions. J. Clim. Appl. Meteorol. 23, 1100–1109. https://doi.org/10.1175/1520-0450(1984)023<1100:TPDSIL>2.0.CO;2.

Baig, M.H.A., Zhang, L., Shuai, T., Tong, Q., 2014. Derivation of a tasselled cap transformation based on Landsat 8 at-satellite reflectance. Remote Sens. Lett. 5, 423–431. https://doi.org/10.1080/2150704X.2014.915434.

Balázs, B., Bíró, T., Dyke, G., Singh, S.K., Szabó, S., 2018. Extracting water-related features using reflectance data and principal component analysis of Landsat images. Hydrol. Sci. J. 63, 269–284. https://doi.org/10.1080/02626667.2018.1425802.

Bijeesh, T.V., Narasimhamurthy, K.N., 2020. Surface water detection and delineation using remote sensing images: a review of methods and algorithms. Sustain. Water Resour. Manag. 6, 68. https://doi.org/10.1007/s40899-020-00425-4.

Bishop, C.M., 2006. Pattern Recognition and Machine Learning. springer.

Bryson, R.A., Hare, F.K., 1974. Climates of North America: Volume 11 of World Survey of Climatology.

Burbach, M.E., Joeckel, R.M., 2006. A delicate balance: rainfall and groundwater in Nebraska during the 2000-2005 drought. Gt. Plains Res. 16, 5–16.

Chen, Xunhong, Chen, Xi, 2004. Simulating the effects of reduced precipitation on ground water and streamflow in the Nebraska sand hills. J. Am. Water Resour. Assoc. 40, 419–430. https://doi.org/10.1111/j.1752-1688.2004.tb01040.x.

Conrad, O., Bechtel, B., Bock, M., Dietrich, H., Fischer, E., Gerlitz, L., Wehberg, J., Wichmann, V., Böhner, J., 2015. System for automated geoscientific analyses (SAGA) v. 2.1. 4. Geosci. Model Dev. Discuss. 8.

Conservation and Survey Division, 2021a. No Title [WWW Document]. CSD Interact. Data Map.

Conservation and Survey Division, 2021b. No Title [WWW Document]. CSD Interact. Data Map. URL http://snr.unl.edu/csd/map/ (accessed 10.20.20).

Cook, B.I., Smerdon, J.E., Seager, R., Coats, S., 2014. Global warming and 21st century drying. Clim. Dyn. 43, 2607–2627. https://doi.org/10.1007/s00382-014-2075-y.

Crist, E.P., Cicone, R.C., 1984. A physically-based transformation of thematic mapper data—the TM tasseled cap. IEEE Trans. Geosci. Remote Sens. GE-22 256–263. https://doi.org/10.1109/TGRS.1984.350619.

Crist, E.P., Kauth, R.J., 1986. The Tasseled Cap de-mystified. [transformations of MSS and TM data].

Dai, A., Trenberth, K.E., Qian, T., 2004. A global dataset of Palmer Drought Severity Index for 1870-2002: relationship with soil moisture and effects of surface warming. J. Hydrometeorol. 5, 1117–1130. https://doi.org/10.1175/JHM-386.1.

Dappen, P., Merchant, J., Ratcliffe, I., Robbins, C., 2007. Delineation of 2005 land use patterns for the state of Nebraska. Lincoln, NE Cent. Adv. L. Manag. Inf. Technol. Sch. Nat. Resour. Univ. Nebraska-Lincoln.

Ding, Y., Hayes, M.J., Widhalm, M., 2011. Measuring economic impacts of drought: a review and discussion. Disaster Prev. Manag. https://doi.org/10.1108/09653561111161752.

Dracup, J.A., 1991. Drought monitoring. Stoch. Hydrol. Hydraul. 5, 261–266. https://doi.org/10.1007/BF01543134.

Du, Z., Linghu, B., Ling, F., Li, W., Tian, W., Wang, H., Gui, Y., Sun, B., Zhang, X., 2012. Estimating surface water area changes using time-series Landsat data in the Qingjiang River Basin, China. J. Appl. Remote Sens. 6, 063609 https://doi.org/10.1117/1.JRS.6.063609.

Dubrovsky, M., Svoboda, M.D., Trnka, M., Hayes, M.J., Wilhite, D.A., Zalud, Z., Hlavinka, P., 2009. Application of relative drought indices in assessing climate-change impacts on drought conditions in Czechia. Theor. Appl. Climatol. 96, 155–171. https://doi.org/10.1007/s00704-008-0020-x.

Frazier, P.S., Page, K.J., 2000. Water body detection and delineation with Landsat TM data. Photogramm. Eng. Remote Sens. 66, 1461–1468.

Getis, A., Ord, J.K., 1992. The analysis of spatial association by use of distance statistics. Geogr. Anal. 24, 189–206. https://doi.org/10.1111/j.1538-4632.1992.tb00261.x.

Gong, Y., Liu, G., Schwartz, F., 2015. Quantifying the response time of a lake–Groundwater interacting system to climatic perturbation. Water 7, 6598–6615. https://doi.org/10.3390/w7116598.

Gosselin, D.C., Rundquist, D.C., McFeeters, S.K., 2000. Remote monitoring of selected ground-water dominated lakes in the Nebraska Sand Hills. J. Am. Water Resour. Assoc. 36, 1039–1051. https://doi.org/10.1111/j.1752-1688.2000.tb05708.x.

Gutentag, E.D., Heimes, F.J., Krothe, N.C., Luckey, R.R., Weeks, J.B., 1984. Geohydrology of the High Plains aquifer in parts of Colorado, Kansas, Nebraska, New Mexico, oklahoma, South Dakota, Texas, and Wyoming (USGS, USA, groundwater). US Geol. Surv. Prof. Pap. https://doi.org/10.3133/pp1400B.

Harris, A.R., 1994. Time series remote sensing of a climatically sensitive lake. Remote Sens. Environ. 50, 83–94. https://doi.org/10.1016/0034-4257(94)90036-1.

Heim, R.R., 2002. A review of twentieth-century drought indices used in the United States. Bull. Am. Meteorol. Soc. 83, 1149–1166. https://doi.org/10.1175/1520-0477-83.8.1149.

Hoan, N.T., Tateishi, R., Phong, D.X., Johnson, B., 2012. Global water mapping using MODIS tasseled cap indexes. In: 2012 IEEE International Geoscience and Remote Sensing Symposium. IEEE, pp. 7161–7164. https://doi.org/10.1109/IGARSS.2012.6352011.

Huang, C., Wylie, B., Yang, L., Homer, C., Zylstra, G., 2002. Derivation of a tasselled cap transformation based on Landsat 7 at-satellite reflectance. Int. J. Remote Sens. 23, 1741–1748.

Huang, S., Dahal, D., Young, C., Chander, G., Liu, S., 2011. Integration of Palmer Drought Severity Index and remote sensing data to simulate wetland water surface from 1910 to 2009 in Cottonwood Lake area, North Dakota. Remote Sens. Environ. 115, 3377–3389. https://doi.org/10.1016/J.RSE.2011.08.002.

Jain, S.K., Singh, R.D., Jain, M.K., Lohani, A.K., 2005. Delineation of flood-prone areas using remote sensing techniques. Water Resour. Manag. 19, 333–347. https://doi.org/10.1007/s11269-005-3281-5.

Jiang, Z., Qi, J., Su, S., Zhang, Z., Wu, J., 2012. Water body delineation using index composition and HIS transformation. Int. J. Remote Sens. 33, 3402–3421. https://doi.org/10.1080/01431161.2011.614967.

Keyantash, J., Dracup, J.A., Keyantash, J., Dracup, J.A., 2002. The quantification of drought: an evaluation of drought indices. Bull. Am. Meteorol. Soc. 83, 1167–1180. https://doi.org/10.1175/1520-0477-83.8.1167.
Kushnir, Y., Seager, R., Ting, M., Naik, N., Nakamura, J., 2010. Mechanisms of tropical atlantic SST influence on North American precipitation variability. J. Clim. 23, 5610–5628. https://doi.org/10.1175/2010JCLI3172.1.
Langbein, W.B., 1961. Salinity and Hydrology of Closed Lakes: A Study of the Long-term Balance Between Input and Loss of Salts in Closed Lakes. US GovernmentPrint. Office.
Li, J., Yang, X., Maffei, C., Tooth, S., Yao, G., 2018. Applying independent component analysis on sentinel-2 imagery to characterize geomorphological responses to an extreme flood event near the non-vegetated Río Colorado Terminus, Salar de Uyuni, Bolivia. Remote Sens. 10, 725. https://doi.org/10.3390/rs10050725.
Liao, J., Shen, G., Li, Y., 2013. Lake variations in response to climate change in the Tibetan Plateau in the past 40 years. Int. J. Digit. Earth 6, 534–549. https://doi.org/10.1080/17538947.2012.656290.
Liu, G., Schwartz, F.W., 2012. Climate-driven variability in lake and wetland distribution across the Prairie Pothole Region: from modern observations to long-term reconstructions with space-for-time substitution. Water Resour. Res. 48 https://doi.org/10.1029/2011WR011539.
MacKay, D.J.C., 1992. Bayesian interpolation. Neural Comput. 4, 415–447. https://doi.org/10.1162/neco.1992.4.3.415.
Mason, I.M., Guzkowska, M.A.J., Rapley, C.G., Street-Perrott, F.A., 1994. The response of lake levels and areas to climatic change. Clim. Change 27, 161–197. https://doi.org/10.1007/BF01093590.
Mo, K.C., Lettenmaier, D.P., 2018. Drought variability and trends over the central United States in the instrumental record. J. Hydrometeorol. 19, 1149–1166. https://doi.org/10.1175/JHM-D-17-0225.1.
Mo, K.C., Schemm, J.-K.E., Yoo, S.-H., 2009. Influence of ENSO and the Atlantic Multidecadal Oscillation on Drought over the United States. J. Clim. 22, 5962–5982. https://doi.org/10.1175/2009JCLI2966.1.
Murphy, K.P., 2012. Machine Learning: a Probabilistic Perspective. MIT press.
National Climatic Data Center, N.O. and A.A, 2020. No Title [WWW Document]. Online Clim. Data. URL https://www.ncdc.noaa.gov/cdo-web/datasets (Accessed 9.22.20).
Nigam, S., Guan, B., Ruiz-Barradas, A., 2011. Key role of the Atlantic Multidecadal Oscillation in 20th century drought and wet periods over the Great Plains. Geophys. Res. Lett. 38 https://doi.org/10.1029/2011GL048650.
Ong, J., 2010. Investigation of spatial and temporal processes of lake-aquifer interactions in the Nebraska Sand Hills. Diss. Theses Earth Atmos. Sci. 13, 314.
Ozesmi, S.L., Bauer, M.E., 2002. Satellite remote sensing of wetlands. Wetl. Ecol. Manag. 10, 381–402. https://doi.org/10.1023/A:1020908432489.
Paul, A., Tripathi, D., Dutta, D., 2018. Application and comparison of advanced supervised classifiers in extraction of water bodies from remote sensing images. Sustain. Water Resour. Manag. 4, 905–919. https://doi.org/10.1007/s40899-017-0184-6.
Pedregosa, F., Varoquaux, G., Gramfort, A., Michel, V., Thirion, B., Grisel, O., Blondel, M., Prettenhofer, P., Weiss, R., Dubourg, V., Vanderplas, J., Passos, A., Cournapeau, D., Brucher, M., Perrot, M., Duchesnay, É., 2011. Scikit-learn: machine learning in Python. J. Mach. Learn. Res. 12, 2825–2830.
Peters, E., Bier, G., van Lanen, H.A.J., Torfs, P.J.J.F., 2006. Propagation and spatial distribution of drought in a groundwater catchment. J. Hydrol. 321, 257–275. https://doi.org/10.1016/j.jhydrol.2005.08.004.
Peterson, S.M., Traylor, J.P., Guira, M., 2020. Groundwater Availability of the Northern High Plains Aquifer in Colorado, Kansas, Nebraska, South Dakota, and Wyoming. U.S. Geological Survey. https://doi.org/10.3133/pp1864.
Pham, S.V., Leavitt, P.R., McGowan, S., Peres-Neto, P., 2008. Spatial variability of climate and land-use effects on lakes of the northern Great Plains. Limnol. Oceanogr. 53, 728–742.
Schubert, S.D., Suarez, M.J., Pegion, P.J., Koster, R.D., Bacmeister, J.T., 2004. Causes of long-term drought in the US Great Plains. J. Clim. 17, 485–503.
Schubert, S., Gutzler, D., Wang, H., Dai, A., Delworth, T., Deser, C., Findell, K., Fu, R., Higgins, W., Hoerling, M., Kirtman, B., Koster, R., Kumar, A., Legler, D., Lettenmaier, D., Lyon, B., Magana, V., Mo, K., Nigam, S., Pegion, P., Phillips, A., Pulwarty, R., Rind, D., Ruiz-Barradas, A., Schemm, J., Seager, R., Stewart, R., Suarez, M., Syktus, J., Ting, M., Wang, C., Weaver, S., Zeng, N., 2009. A U.S. Clivar project to assess and compare the responses of global climate models to drought-related SST forcing patterns: overview and results. J. Clim. 22, 5251–5272. https://doi.org/10.1175/2009JCLI3060.1.
Scott, L.M., Janikas, M.V., 2010. Spatial statistics in ArcGIS. Handbook of Applied Spatial Analysis. Springer, Berlin Heidelberg, pp. 27–41. https://doi.org/10.1007/978-3-642-03647-7_2.
Smith, A.J., Townley, L.R., 2002. Influence of regional setting on the interaction between shallow lakes and aquifers. Water Resour. Res. 38 https://doi.org/10.1029/2001wr000781, 10-1-10–13.
Stehman, S.V., 1997. Selecting and interpreting measures of thematic classification accuracy. Remote Sens. Environ. 62, 77–89. https://doi.org/10.1016/S0034-4257(97)00083-7.
Szilagyi, J., Zlotnik, V.A., Gates, J.B., Jozsa, J., 2011. Mapping mean annual groundwater recharge in the Nebraska Sand Hills, USA. Hydrogeol. J. 19, 1503–1513. https://doi.org/10.1007/s10040-011-0769-3.
Tague, C., Grant, G., Farrell, M., Choate, J., Jefferson, A., 2008. Deep groundwater mediates streamflow response to climate warming in the Oregon Cascades. Clim. Change 86, 189–210. https://doi.org/10.1007/s10584-007-9294-8.
Tang, L., Duan, X., Kong, F., Zhang, F., Zheng, Y., Li, Z., Mei, Y., Zhao, Y., Hu, S., 2018. Influences of climate change on area variation of Qinghai Lake on Qinghai-Tibetan Plateau since 1980s. Sci. Rep. 8, 1–7. https://doi.org/10.1038/s41598-018-25683-3.
Tian, S., Zhang, X., Tian, J., Sun, Q., 2016. Random forest classification of wetland landcovers from multi-sensor data in the arid region of Xinjiang, China. Remote Sens. (Basel) 8, 954. https://doi.org/10.3390/rs8110954.
Tweed, S., Leblanc, M., Cartwright, I., 2009. Groundwater–surface water interaction and the impact of a multi-year drought on lakes conditions in South-East Australia. J. Hydrol. 379, 41–53. https://doi.org/10.1016/j.jhydrol.2009.09.043.
Vermote, E., Justice, C., Claverie, M., Franch, B., 2016. Preliminary analysis of the performance of the Landsat 8/OLI land surface reflectance product. Remote Sens. Environ. 185, 46–56. https://doi.org/10.1016/j.rse.2016.04.008.
Wang, C., Jia, M., Chen, N., Wang, W., 2018a. Long-term surface water dynamics analysis based on landsat imagery and the google earth engine platform: a case study in the Middle Yangtze River Basin. Remote Sens. 10, 1635. https://doi.org/10.3390/rs10101635.
Wang, J., Song, C., Reager, J.T., Yao, F., Famiglietti, J.S., Sheng, Y., MacDonald, G.M., Brun, F., Schmied, H.M., Marston, R.A., Wada, Y., 2018b. Recent global decline in endorheic basin water storages. Nat. Geosci. 11, 926–932. https://doi.org/10.1038/s41561-018-0265-7.
Wang, Y., Li, Z., Zeng, C., Xia, G.S., Shen, H., 2020. An urban water extraction method combining deep learning and google earth engine. IEEE J. Sel. Top. Appl. Earth Obs. Remote Sens. 13, 768–781. https://doi.org/10.1109/JSTARS.2020.2971783.
White, W.B., Gershunov, A., Annis, J., 2008. Climatic influences on midwest drought during the twentieth century. J. Clim. 21, 517–531. https://doi.org/10.1175/2007JCLI1465.1.
Williamson, C.E., Dodds, W., Kratz, T.K., Palmer, M.A., 2008. Lakes and streams as sentinels of environmental change in terrestrial and atmospheric processes. Front. Ecol. Environ. https://doi.org/10.1890/070140.
Winter, T.C., 1986. Effect of ground-water recharge on configuration of the water table beneath sand dunes and on seepage in lakes in the sandhills of Nebraska. U.S. A. J. Hydrol. 86, 221–237. https://doi.org/10.1016/0022-1694(86)90166-6.
Xu, H., 2006. Modification of normalised difference water index (NDWI) to enhance open water features in remotely sensed imagery. Int. J. Remote Sens. 27, 3025–3033. https://doi.org/10.1080/01431160600589179.
Yan, L., Zheng, M., 2015. The response of lake variations to climate change in the past forty years: A case study of the northeastern Tibetan Plateau and adjacent areas, China. Quat. Int. 371, 31–48. https://doi.org/10.1016/j.quaint.2014.12.057.

Zhang, B., Schwartz, F.W., Liu, G., 2009. Systematics in the size structure of prairie pothole lakes through drought and deluge. Water Resour. Res. 45 https://doi.org/10.1029/2008WR006878.

Zhuang, Y., Chen, C., 2018. A method for water body extraction based on the tasselled cap transformation from remote sensing images. 5th International Workshop on Earth Observation and Remote Sensing Applications, EORSA 2018 - Proceedings. https://doi.org/10.1109/EORSA.2018.8598605.

Zlotnik, V.A., Olaguera, F., Ong, J.B., 2009. An approach to assessment of flow regimes of groundwater-dominated lakes in arid environments. J. Hydrol. 371, 22–30. https://doi.org/10.1016/j.jhydrol.2009.03.012.